nature physics

SUPPLEMENTARY INFORMATION

https://doi.org/10.1038/s41567-019-0672-8

In the format provided by the authors and unedited.

Light emission based on nanophotonic vacuum forces

Nicholas Rivera[1]*, Liang Jie Wong[2,3], John D. Joannopoulos[1], Marin Soljačić[1] and Ido Kaminer[4]*

[1]Department of Physics, Massachusetts Institute of Technology, Cambridge, MA, USA. [2]Singapore Institute of Manufacturing Technology, Singapore, Singapore. [3]School of Electrical and Electronic Engineering, Nanyang Technological University, Singapore, Singapore. [4]Department of Electrical Engineering, Technion, Haifa, Israel. *e-mail: nrivera@mit.edu; kaminer@technion.ac.il

Light emission based on nanophotonic vacuum forces: Supplementary Information

Nicholas Rivera[1], Liang Jie Wong[2,3], John D. Joannopoulos[1], Marin Soljačić[1], and Ido Kaminer[4]

[1]*Department of Physics, Massachusetts Institute of Technology, Cambridge, MA 02139, USA.*

[2]*Singapore Institute of Manufacturing Technology, Singapore 138634, Singapore.*

[3]*School of Electrical and Electronic Engineering, Nanyang Technological University, 50 Nanyang Ave, Singapore 639798.*

[4]*Department of Electrical Engineering, Technion, Haifa 32000, Israel.*

Contents

1 Supplementary Figures

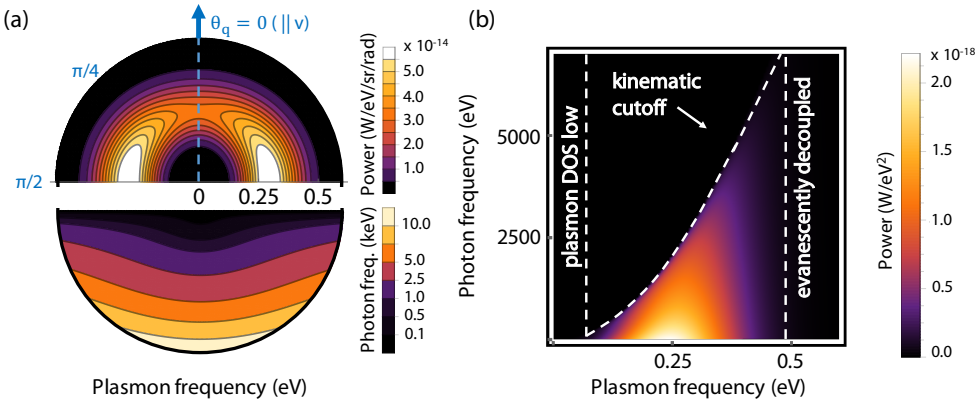

Figure S1: **Correlations between infrared polaritons and X-ray photons in photon-polariton pair emission.** Same as Figure 3 of the main text, except that the electron now travels 10 nm away from the surface of the graphene sheet, and it is doped to a Fermi energy of 0.25 eV.

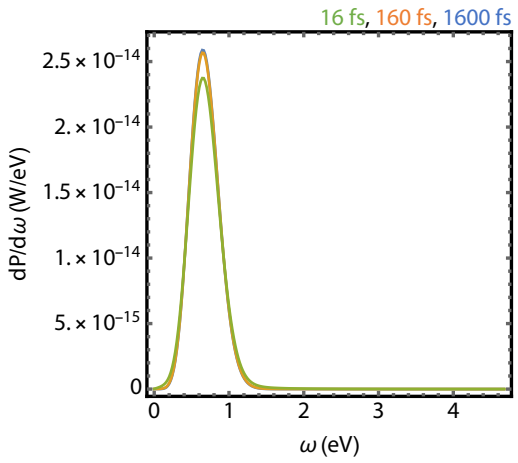

Figure S2: **Influence of Drude losses on photon emission.** Emitted power (into photons) per unit frequency of polaritons for the case of an electron of velocity $0.99c$ traveling 5 nm away from a sheet of Drude graphene doped to a Fermi level of 0.5 eV for Drude relaxation times of 1600 fs, 160 fs, and 16 fs. The Drude time has a weak influence on the emitted power.

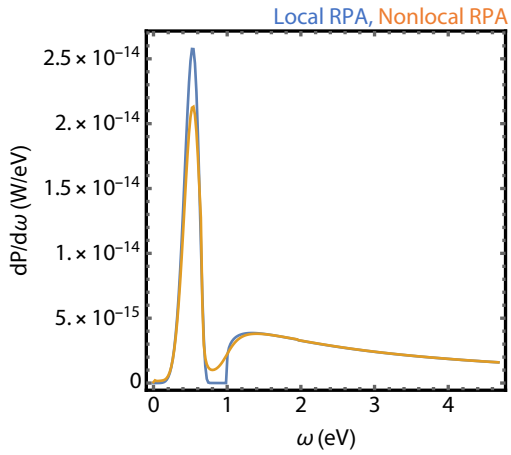

Figure S3: **Influence of interband damping on photon emission.** Emitted power (into photons) per unit frequency of polaritons for the case of an electron of velocity $0.99c$ traveling 5 nm away from a sheet of graphene doped to a Fermi level of 0.5 eV with a Drude relaxation time of 1600 fs. Graphene is modeled here through both the local and nonlocal RPA. Interband damping has a stronger influence on the emitted power, which stays in the same order of magnitude. The power emitted is about 15 fW, compared to 12 fW in the Drude case.

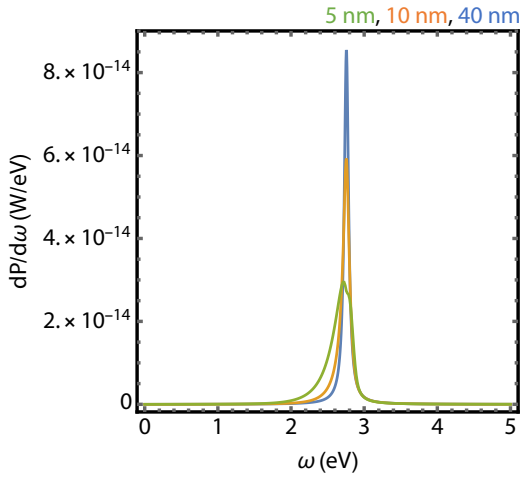

Figure S4: **Photon-polariton emission for electrons near gold films.** Emitted power (into photons) per unit frequency of polaritons for the case of an electron of velocity $0.99c$ traveling 5 nm away from a thin film of Drude gold of varying thicknesses. The underlying emission power stays similar to the case of Fig. S3, varying from 9.9 fW per electron for 40 nm gold to 11 fW per electron for 5 nm gold.

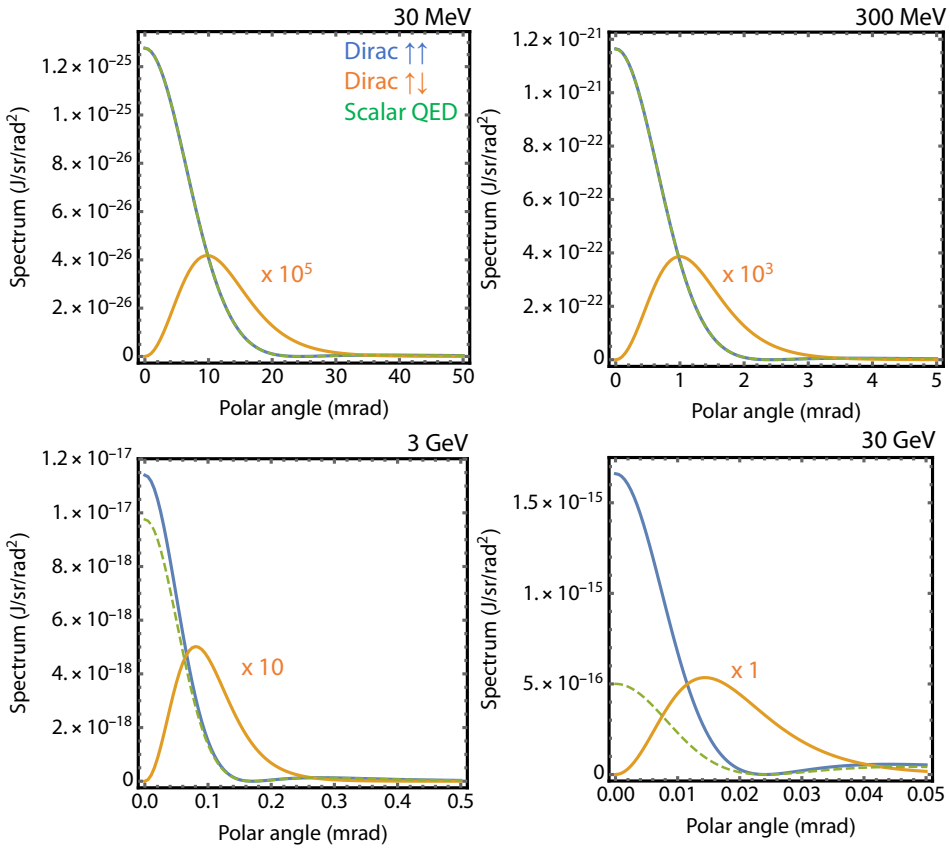

Figure S5: **Influence of the electron spin on photon-polariton pair emission.** Emitted power (into photons) per unit photon angle, plasmon frequency, and plasmon angle in scalar QED versus fermion QED. The contribution to the emission in fermion QED from transitions that conserve the electron spin is shown in blue. Spin-flipping contributions are shown in orange, and the scalar QED prediction is shown in green. The plasmon is emitted in the direction of the electron motion with frequency equal to the Fermi energy of 0.5 eV. The electron is assumed to travel 5 nm away from the surface of graphene. The electron energies considered are 30 MeV (top left), 300 MeV (top right), 3 GeV (bottom left), and 30 GeV (bottom right). As these plots show, the scalar QED results are in excellent agreement with the spin-conserving results of fermion QED for electron kinetic energies below 3 GeV, and continue to predict similar trends as a function of polar angle even at larger electron energies.

2 Experimental considerations for realizing photon-polariton pair emission

In this section, we briefly discuss a few considerations important to experimentally realizing the photon-polariton pair emission effect discussed in this work. We discuss (a) the rate of photon emission associated with photon-polariton pair emission for a realistic electron beam, as achievable by a transmission electron microscope, (b) comparison to other high-energy light sources that are driven by electromagnetic fields, and (c) mitigation of X-ray producing background effects associated with the electron beam impinging the sample.

Photon emission rates The characteristic photon emission rates per electron are on the order of 10^2-10^4 photons per second per electron, for electrons traveling 1-10 nm above the graphene sheet, and a graphene Fermi level between 0.1-1 eV. The corresponding emission length is on the order of 10-1000 km. These numbers are similar to other compact lab-scale photon sources based on high-energy electrons, as can be verified directly from the Larmor formula for a typical example of 5 MeV electrons interacting with 100 MV/m electric fields to produce keV frequency photons. The fact that both the emitted power and the average photon energy scale as γ^2 allows us to infer that the photon emission rate (given by emitted power divided by photon energy) is somewhat insensitive to electron energy. For electron beam currents of 100 nA to 100 μA and an interaction length of 100 μm, the expected rate of photon emission for electrons 5 nm from the surface is about $10^3 - 10^6$ photons per second, the higher values in this range being comparable to X-ray yields from high-harmonic generation[1]. Our scheme also has an advantage that with increasing electron energy, the brightness can be improved, and harder X-rays or even gamma ray energies

could eventually be reached. With multilayer structures[2], and pre-bunching via emittance exchange techniques[3,4], laser-plasma interactions[5], or electromagnetic intensity gratings[6], the photon yields, and spectral brightness can be scaled up by several orders of magnitude.

Comparison to x-ray sources based on strongly excited plasmons We mention one other point of comparison with regards to the emitted power. Consider an electron interacting with an externally pumped graphene plasmon, with a surface field strength of 1 GV/m as was proposed in Ref. [7]; the excitation is approximately monochromatic and can be described by a single plasmon mode. Let us assume that the plasmon frequency is 0.8 eV and that its confinement factor is 100 so that plasmon wavelength is 15 nm. The time-averaged radiation power as a result of an electron scattering off this plasmon mode, calculated through the Larmor formula, is 1.3 nW - about the same value as the *spontaneously* generated power in a photon-polariton pair emission. This is surprising given that a 1 GV/m field in the stimulated emission case corresponds to a large number of plasmons, whereas the spontaneous pair-emission we present here does not involve any driving plasmons. For instance, a 50 nm $\times$ 50 nm excitation area already requires 1000 plasmons to support a 1 GV/m field. This unexpected result – that spontaneous pair-emission can produce as much radiated power as a stimulated emission scenario that uses a large number of plasmons – is explained by the fact that the electron in the spontaneous pair-emission case is "driven" by a highly multi-mode field and experiences the field of effectively half of a polariton for each mode (as a result of the zero-point polariton energy being half the energy of a polariton). The outgoing radiation is consequently also much more spectrally broad compared to the single-mode case.

Mitigation of background effects Regarding background effects (particularly, background effects that produce X-rays) from the electron crossing the sample, the experimental capabilities needed to minimize such effects are present. For example, it is not uncommon in transmission electron microscopes to have an electron beam of size below one nanometer. It is also possible to keep the beam divergence small, such that after about 10-100 microns of propagation (characteristic sample size), the divergence is on the order of a few nanometers. At that level of divergence, most of the electron beam will not penetrate the sample. Background effects can be even further minimized by using porous substrates or by using suspended 2D materials, such as graphene, or hexagonal boron nitride, which can be produced. In this case, there is as high a vacuum-to-solid ratio as possible, and the electrons spend most of their time interacting with vacuum fluctuations. Yet another interesting approach being actively developed, which could be used to both minimize background effects, as well as maximize the X-ray signal from this process, is to use flat electron beams with a very high aspect ratio[8–10]. Low-emittance electron beams of aspect ratios of 100 have been realized experimentally[9]. Such an approach would not only allow the electrons to exist in the nanometer vicinity of the sample surface with minimal spread, but the number of electrons interacting with the sample could be further enhanced. Another consideration for experimental verification, particularly in graphene, is that graphene is not perfectly flat, which will average the spectrum over the distribution of distances between the electron and the graphene surface. Although graphene is known to be not perfectly flat, these "defects" can occur at sufficiently low densities, such that the average height of the electron above the graphene surface is only changed by an amount on the order of a percent[11,12], leading to photon-polariton pair emission with similar

intensity (different by a few percent). With rapid advancement in graphene fabrication techniques, new methods to smoothen wrinkles in graphene continue to emerge, based on the use of boron nitride substrates[13], or paraffin-based transfer[14], both of which can lead to highly smooth graphene. Additionally, given the high resolution of transmission electron microscopes, a preferred area of interaction could be chosen so that such effects can be further mitigated.

3 Fluctuational theory of high energy emission by electrons near photonic structures

In the remainder of this Supplement, we derive in detail the theory of two-photon emission by a free electron moving through an arbitrary photonic structure. First (Sections 3 and 4), we develop a "fluctuational theory", in which we treat the two-photon emission process as effectively a one-photon process, in which the vacuum fluctuations of a photonic structure act as an external field which scatters the electron, leading to far-field photon emission. Then (Section 5), we then develop a more direct theory of the two-photon process by calculating simultaneous emission of a low-energy photon in the photonic structure and a high-energy photon, within the framework of relativistic quantum field theory. We from now on refer to the low-energy photon in the photonic structure as a "polariton", as the nontrivial spatial and spectral properties of photons in complex structures arise from the complex interplay of electromagnetic fields with polarization charges and currents (i.e., matter). We conclude by showing that these two theories make the same predictions and exemplify it with the specific case of the polariton being a plasmon polariton of a two-dimensional electron gas. We explain why the fluctuational theory and the direct theory should be equivalent for any structure.

We consider an electron moving near a nanophotonic structure. Due to electromagnetic fluctuations of the photonic structure, the electron on average feels a mean-square driving field and may radiate either back into the structure or into the far field. Here, we focus specifically on the case in which the electron radiates into the far-field, as we are interested in the spectrum of hard-UV, X-ray, and gamma ray photons emitted by a relativistic electron. At these frequencies, the material response is negligible.

To develop this theory, we first review a general expression from electrodynamics relating far-field radiation to the acceleration of moving charges. Then from relativistic mechanics, we parameterize the acceleration of the charge in terms of a driving field. Last we find the driving field associated with electromagnetic vacuum fluctuations in the material. This way, we relate the far-field radiation to the vacuum fluctuations that oscillate the electron. These steps lead to a general expression allowing one to determine the far-field radiation at any frequency, by charged particles of any velocity, induced by quantum vacuum fluctuations in any photonic structure.

Radiation by a moving charge The time-averaged power P per unit solid angle Ω, $\frac{dP}{d\Omega}$, emitted by a system of charges at a position $\mathbf{R}$, far from the origin of coordinates, is related to the time-averaged Poynting vector $\mathbf{S}$ by $\frac{dP}{d\Omega} = R^2\hat{n}\cdot\mathbf{S}$, where $\hat{n}$ is the unit vector in the direction of observation. Expressing the time-dependent fields in Fourier domain using the convention $\mathbf{E}(\mathbf{r},t) = \int_{-\infty}^{\infty} d\omega'\ e^{-i\omega' t}\mathbf{E}(\mathbf{r},\omega')$, the single-sided (positive-frequency) time-averaged energy U radiated per unit frequency ω' per unit solid angle can be written as

$$\frac{dU}{d\omega' d\Omega} = \frac{4\pi R^2}{\mu_0}\hat{n}\cdot \text{Re}\,[\mathbf{E}(\mathbf{r},\omega')\times\mathbf{B}^*(\mathbf{r},\omega')], \tag{S1}$$

where μ_0 is the permeability of free space. From Maxwell's equations in the far-field, we have that the frequency-domain magnetic field is related to the frequency-domain electric field by $\mathbf{B}(\mathbf{r},\omega') = \frac{\hat{n}}{c} \times \mathbf{E}(\mathbf{r},\omega')$, meaning that we may write Equation (S1) purely in terms of $\mathbf{E}(\mathbf{r},\omega')$ as

$$\frac{dU}{d\omega' d\Omega} = \frac{4\pi R^2}{\mu_0 c}\left(\left|\mathbf{E}(\mathbf{r},\omega')\right|^2 - \left|\hat{n}\cdot\mathbf{E}(\mathbf{r},\omega')\right|^2\right) = \frac{4\pi R^2}{\mu_0 c}\left|\mathbf{E}(\mathbf{r},\omega')\right|^2, \tag{S2}$$

where the last equality applies when only the radiative component is considered.

We now consider the specific case of the fields of a moving electron of charge $-e$ with a general trajectory corresponding to position $\mathbf{r}(t)$ and velocity $\dot{\mathbf{r}}(t) = \mathbf{v}(t) = c\boldsymbol{\beta}(t)$, with c the speed of light. From the Lienard-Wiechert potentials[15], the frequency-domain electric field of the moving electron is given by

$$\mathbf{E}(\mathbf{r},\omega') = \int \frac{dt'}{2\pi}\, e^{i\omega' t'} \frac{-e}{4\pi\epsilon_0 Rc(1-\hat{n}\cdot\boldsymbol{\beta}(t'))^3}\left(\hat{n}\times\left((\hat{n}-\boldsymbol{\beta}(t'))\times\dot{\boldsymbol{\beta}}(t')\right)\right), \tag{S3}$$

where ϵ_0 is the permittivity of free space. We note that in this expression, a primed time variable denotes the retarded time of the electron for the observer at distance R and is given by $t' = t - \frac{R(t)}{c}$. Time-derivatives are calculated with respect to t'. We can change the integration variable in (S3) to the non-retarded time t by making a change of variables $t' = t(1-\hat{n}\cdot\boldsymbol{\beta})$. Plugging Equation (S3) into Equation (S2) yields a general expression connecting the acceleration of the electron to the far-field radiation spectrum.

In physical situations involving radiation by accelerated electrons[16], it is common for the modulation of the electron trajectory by a driving field to be very weak, meaning that deviations of the electron from an initial straight line motion in the absence of a driving field are small. This

is also the case in all cases considered in this manuscript, in which the driving fields are quantum fluctuations of a nanophotonic vacuum. Thus, we approximate (S3) to lowest order in the electron modulation by taking $(1-\hat{n}\cdot\boldsymbol{\beta}(t'))\approx(1-\hat{n}\cdot\boldsymbol{\beta})$ and $\hat{n}-\boldsymbol{\beta}(t')\approx\hat{n}-\boldsymbol{\beta}$, where $\boldsymbol{\beta}$ without explicit time-dependence represents the initial velocity of the electron, normalized to c. Applying this approximation, the angular and frequency spectrum of radiation is given by

$$\frac{dU}{d\omega' d\Omega}=\frac{e^2}{16\pi^3\epsilon_0 c(1-\beta\cos\theta)^4}\left|\int dt\, e^{-i\omega'(1-\beta\cos\theta)t}\hat{n}\times\left((\hat{n}-\boldsymbol{\beta})\times\dot{\boldsymbol{\beta}}(t)\right)\right|^2, \tag{S4}$$

where $\theta=\cos^{-1}\left(\hat{n}\cdot\hat{\beta}\right)$ is the angle of radiation emission relative to the initial direction of electron motion $\hat{\beta}=\frac{\boldsymbol{\beta}}{\beta}$ (with β the magnitude of $\boldsymbol{\beta}$). Small deviations of the trajectory $R(t)$ from the unperturbed linear trajectory are neglected in the exponential, as such corrections yield corrections at second-order in the trajectory modulation. We have also replaced the quantity inside the modulus-squared by its complex conjugate, without loss of generality, for reasons that will be apparent later. We now proceed to relate the normalized acceleration $\dot{\boldsymbol{\beta}}(t)$ to external fields that the electron experiences.

Modulation of the trajectory of a charged particle by an electromagnetic field Consider external (driving) electric and magnetic fields $\mathbf{E}$ and $\mathbf{B}$. The acceleration of the electron of mass m is governed by the Newton-Lorentz equation of motion:

$$mc(\gamma(t)\dot{\boldsymbol{\beta}}(t))=-e[\mathbf{E}(t)+c\boldsymbol{\beta}(t)\times\mathbf{B}(t)], \tag{S5}$$

where the Lorentz factor $\gamma(t)=(1-\beta^2(t))^{-1/2}$ accounts for the electron's relativistic motion. As in the previous section, we apply the approximation that the trajectory of the electron is weakly perturbed from its initial trajectory $\mathbf{r}(t)=\mathbf{r}_0+\mathbf{v}t$. In this case, we may assume that $\gamma(t)$ is de-

termined only by the velocity component parallel to $\mathbf{v}$. Taking this velocity component without loss of generality to be along the z-direction of a Cartesian system of coordinates, we approximate $\gamma(t) \approx (1-\beta_z^2(t))^{-1/2}$. In expressions where we do not take its time derivative, it can be approximated as constant: $\gamma \approx (1-\beta^2)^{-1/2}$, where functions without explicit time-dependence represent initial values. In that case, Newton's equations of motion for the z-directed velocity can be shown to reduce to:

$$\dot{\beta}_z(t) = -\frac{e}{\gamma^3 mc} E_z(t). \tag{S6}$$

For components of the acceleration perpendicular to the initial velocity, the equation of motion reduces to

$$\dot{\boldsymbol{\beta}}_\perp(t) = -\frac{e}{\gamma mc}\left(\mathbf{E}_\perp(t) + (\mathbf{v}\times\mathbf{B}(t))_\perp\right). \tag{S7}$$

In what follows, we make our final approximation with regards to the electron motion, which is that the driving fields we consider are quasi-electrostatic and approximately satisfy the Laplace equation. As such, the magnetic part of the quasi-static field is neglected. This approximation is justified when the electromagnetic driving field is highly spatially confined, meaning that the length scale of the spatial variations of the field λ, are much smaller than the free-space wavelength of light, $\lambda = \frac{2\pi c}{\omega}$, at the same frequency ω (i.e., $\lambda \ll \frac{2\pi c}{\omega}$). This approximation is accurate in the systems we consider, because such highly confined fields are also advantageous for generating X-rays and gamma rays with relatively low energy electrons[7]. In that case, the acceleration is completely specified in terms of the electric field as $\dot{\boldsymbol{\beta}}(t) = -\frac{e}{\gamma mc}\left(\mathbf{E}_\perp(t), \frac{E_z(t)}{\gamma^2}\right) \equiv -\frac{e}{\gamma mc}\mathbf{E}_\gamma(t)$.

Plugging this expression for the acceleration into Equation (S4) yields

$$\frac{dU}{d\omega' d\Omega} = \frac{e^4 T_{ij} T_{ik}}{16\pi^3 \epsilon_0 m^2 \gamma^2 c^3 (1-\beta\cos\theta)^4} \int dt dt' \; e^{-i\omega'(1-\beta\cos\theta)(t-t')} E_{\gamma,j}(\mathbf{r}(t)) E_{\gamma,k}(\mathbf{r}(t')), \quad \text{(S8)}$$

where for brevity, we have defined the tensor T_{ij} as the ij-component of linear operation $\hat{n} \times ((\hat{n} - \boldsymbol{\beta})\times)$, and we are using Einstein repeated-index notation.

Having parameterized the far-field radiation in terms of the driving field, we now consider a situation in which this driving field is a fluctuating field of a nanophotonic structure in thermal equilibrium, so that the fluctuations are Bose-Einstein distributed in frequency. These fluctuations have both a quantum component and a thermal component. Only the quantum component persists at zero temperature. To find the average power radiated by electrons in this fluctuating field, we take the (quantum) ensemble average of Equation (S8) over all realizations of the field. The resulting "master formula" connecting fluctuating electric fields to far-field radiation is then:

$$\frac{d\langle U\rangle}{d\omega' d\Omega} = \frac{e^4 T_{ij} T_{ik}}{16\pi^3 \epsilon_0 m^2 \gamma^2 c^3 (1-\beta\cos\theta)^4} \int dt dt' \; e^{-i\omega'(1-\beta\cos\theta)(t-t')} \langle E_{\gamma,j}(\mathbf{r}(t)) E_{\gamma,k}(\mathbf{r}(t'))\rangle, \quad \text{(S9)}$$

where $\langle(\cdots)\rangle$ is the ensemble average of $(\cdots)$. To complete the fluctuational theory of photon-polariton pair emission, we require the ensemble average of a product of two electric fields in the vacuum state of an arbitrary photonic structure. From the quantum theory of the macroscopic electromagnetic field, one finds that such an ensemble average is given by:

$$\langle E_i(\mathbf{r},t) E_j(\mathbf{r}',t')\rangle = \frac{\hbar}{\pi\epsilon_0 c^2} \int_0^\infty d\omega \; \omega^2 \text{Im}\, G_{ij}(\mathbf{r},\mathbf{r}',\omega) \left(n_\omega e^{i\omega(t-t')} + (n_\omega + 1) e^{-i\omega(t-t')} \right), \quad \text{(S10)}$$

where $\hbar$ is the reduced Planck constant, G_{ij} is the Dyadic Green's function of the medium, and $n_\omega = (e^{\frac{\hbar\omega}{kT}} - 1)^{-1}$ is a Bose-Einstein occupation factor evaluated at temperature T.

Given the result of Equation (S10), Equation (S9) can be expressed as:

$$\frac{dU}{d\omega' d\Omega} = \frac{e^4\hbar}{16\pi^4\epsilon_0^2 m^2 c^5 \gamma^2 (1-\beta\cos\theta)^4} T_{ij}T_{ik} \times \int dt dt' \int_0^\infty d\omega\, \omega^2 e^{-i\omega'(1-\beta\cos\theta)(t-t')} \text{Im}\, G_{\gamma,jk}(\mathbf{r}(t),\mathbf{r}(t'),\omega) \left(n_\omega e^{i\omega(t-t')} + (n_\omega+1)e^{-i\omega(t-t')}\right), \tag{S11}$$

where $G_{\gamma,jk}$ differs from G_{jk} by a factor of γ^{-2} if one component is along z, and by a factor of γ^{-4} if both components are along z. In other words: $G_{\gamma,jk} = c_j c_k G_{jk}$, where $c_j = \gamma^{-2}$ if j refers to the z-component, and $c_j = 1$ otherwise. We have reintroduced here the convention that repeated indices are summed. Equation (S11) can be written in a more compact form for material systems which are reciprocal. In particular, Equation (S11) can be re-expressed as

$$\frac{dU}{d\omega' d\Omega} = \frac{e^4\hbar}{16\pi^4\epsilon_0^2 m^2 c^5 \gamma^2 (1-\beta\cos\theta)^4} \int dt dt' d\omega\, \omega^2 \Theta(\omega) \text{Im}\left[e^{-i\omega'(1-\beta\cos\theta)(t-t')} \left(n_\omega e^{i\omega(t-t')} + (n_\omega+1)e^{-i\omega(t-t')}\right) \text{tr}\left[\mathbf{T}\mathbf{G}(\mathbf{r}(t),\mathbf{r}(t'),\omega)\mathbf{T}^{\mathrm{T}}\right]\right], \tag{S12}$$

where bolded versions of quantities that originally had indices denote matrices. Additionally, we have included a Heaviside step function ($\Theta(\omega) = 1$ if $\omega > 0$ and $\Theta(\omega) = 0$ otherwise) to extend the domain of the frequency integration from $-\infty$ to ∞.

Before proceeding to evaluate these expressions for specific material systems, we comment that the replacement of deterministic fields by their quantum averages is a key step in any calculation in the framework of fluctuational electrodynamics (see for example Refs. [17–21] and references therein). This framework has thus far been used to predictively calculate phenomena such as near- and far-field heat transfer, Casimir forces, Casimir-Polder and van der Waals forces. In what fol-

lows, we briefly describe how the concept that led us to Equation (S9) has been used to develop successful theories of Casimir forces and near-field radiative heat transfer.

Within fluctuational electrodynamics, the step that led to Equation (S9) (constructing a classical model, and then taking quantum averages), is ubiquitous. For example, this step is used in Casimir force between two polarizable bodies. In the calculation, one calculates the classical Lorentz force felt by a polarizable structure due to a field[21,22]. The expression for the Lorentz force becomes an expression in terms of the permittivity and permeability of the structure, as well as the (vacuum) fields felt by the structure. Then, to account for the fluctuating nature of the fields that generate Casimir forces, one replaces the fields by their ensemble average in the electromagnetic vacuum. In another example of such a replacement of fields by their ensemble averages, when one is interested in radiative heat transfer between two bodies, one calculates the Poynting flux over the surface of a body due to fluctuating currents in the bodies, and then replaces the fields by their ensemble average taking into account the finite temperatures of the bodies[19].

We also briefly comment about the physical significance of the n_ω and $n_\omega + 1$ factors. The term which has n_ω represents physically a situation in which a polariton (i.e., low frequency photon of the photonic structure) at frequency ω is absorbed, while the term with $n_\omega + 1$ represents emission of a polariton. When $n_\omega = 0$, as is the case at zero-temperature, only the "1" contribution remains, which by the general principles of quantum mechanics, corresponds to the spontaneous emission of a polariton. The photon emission at frequency ω' is already spontaneous, as it is considered in the absence of additional photons at frequency ω'. It therefore follows that at zero

temperature, *the emission due to vacuum fluctuations derived here corresponds to a two-quanta spontaneous emission process in which a photon and a polariton are emitted.* When $n_\omega \gg 1$, both terms contribute approximately equally, resulting in a combined effect of stimulated emission and absorption. Together, they reproduce the classical effect of polariton-driven (inverse) Compton radiation as was derived classically in[7]. This match further corroborates our findings in these formulas. Furthermore, in the final section of the SM we derive results equivalent to those of Equation (S12) at zero temperature from a direct application of Fermi's golden rule, without using any classical or fluctuational electrodynamics arguments. To summarize this section, Formula (S25) produces both the two-photon emission and inverse-Compton scattering, both at zero temperature and at a finite temperature. Formula (S12) may be seen as the master formula for any future calculation which seeks to understand fluctuation-induced far-field emission from free electrons.

4 Application to a planar interface

We now consider the case when the electromagnetic quantum fluctuations that interact with a relativistic electron are those of a structure with translational invariance in two dimensions. For simplicity, we also consider the case in which the electron flies parallel to the plane of translational invariance, defined as the yz-plane. For the example of a thin film of thickness d with permittity $\epsilon(\omega)$ surrounded by infinite dielectric of permittivities ϵ_1 ($x > d/2$) and ϵ_2 ($x < -d/2$), the Green's function above the slab (in the ϵ_1 region) can be written as as a sum of contributions from p- and s-polarized plane waves as[21]:

$$G_{ij}(\mathbf{r},\mathbf{r}',\omega) = \frac{i}{2}\int \frac{d^2q}{(2\pi)^2}\,\left(C_{ij}^{p}(\mathbf{q},\omega) + C_{ij}^{s}(\mathbf{q},\omega)\right) e^{i\mathbf{q}\cdot(y-y',z-z')} e^{-\kappa_q(x+x')}, \tag{S13}$$

where $\kappa_q = \sqrt{q^2 - \epsilon_1 \frac{\omega^2}{c^2}}$, and $C_{ij}^{p,s}(\mathbf{q}, \omega)$ are tensors that take into account the differences in polarizations and reflectivities of p- and s- polarized waves[21]. The strength of contributions from p- and s- polarized waves differs substantially in the near-field zone (i.e., high wavenumbers q) where $\frac{cq}{\omega} \gg 1$. In particular, p- polarized contributions dominate by a factor of $\left(\frac{cq}{\omega}\right)^2$, as shown in[23–25]. As we are interested in high-frequency radiation, which we will show (in Equation (S21)) comes from high-wavevector polariton modes, we may approximate the Green's function by its p-polarized part in the electrostatic limit, with $C_{ij}^{p}(\mathbf{q}, \omega)$ given by

$$C_{ij}^{p}(\mathbf{q}, \omega) = -2i \frac{c^2 q}{\omega^2} r_p(\mathbf{q}, \omega) \hat{\epsilon}_i(\mathbf{q}) \hat{\epsilon}_j^*(\mathbf{q}), \tag{S14}$$

with $\hat{\epsilon}(\mathbf{q}) \equiv \frac{\hat{q} + i\hat{x}}{\sqrt{2}}$ and $r_p(\mathbf{q}, \omega)$ being the reflectivity of a p- polarized wave of wavevector $\mathbf{q}$ and frequency ω. Thus, for a general planar interface, treated in the electrostatic limit, the radiated photon spectrum is given by (substituting Equations (S13) and (S14) into (S12))

$$\frac{1}{T_0} \frac{d\langle U \rangle}{d\omega' d\Omega} = \frac{e^4 \hbar}{8\pi^3 \epsilon_0^2 m^2 c^3 \gamma^2 (1 - \beta \cos\theta)^4} \int \frac{d^2 q}{(2\pi)^2} d\omega \; \theta(\omega) q |\mathbf{T} \hat{\epsilon}_\gamma(\mathbf{q})|^2 \text{Im}\; r_p(\mathbf{q}, \omega) e^{-2qx_0} \times$$
$$(n_\omega \delta(\omega'(1 - \beta \cos\theta) - q_z v - \omega) + (n_\omega + 1) \delta(\omega'(1 - \beta \cos\theta) - q_z v + \omega)) \tag{S15}$$

where $\hat{\epsilon}_\gamma(\mathbf{q}) = \frac{1}{\sqrt{2}}(i, \sin\chi_{\mathbf{q}}, \frac{\cos\chi_{\mathbf{q}}}{\gamma^2})$, T_0 is the interaction time, β is the magnitude of the velocity, $\chi_{\mathbf{q}}$ is the angle made by $\mathbf{q}$ to the z-axis, and x_0 is the position of the electron in the x-direction, transverse to the sheet. Henceforth, although we assume a finite temperature, and so $n_\omega \neq 0$, no explicit reference to variables involving temperature will be made. The dependence on temperature of the expressions was explained in the previous section. Additionally, since $\frac{d\langle U \rangle}{T_0}$ has the dimensions of power, we will now refer to it as dP (with no angle brackets, for brevity).

We note that the assumptions in writing the Green's function can straightforwardly be gen-

eralized beyond the electrostatic limit, which means including s-polarized contributions as well as including retardation effects (i.e., effects from $q \sim \frac{\omega}{c}$) in the the p- polarized contributions. When doing this, one must remember that the electrostatic limit was also employed in deriving Equation (S9), where magnetic forces have been neglected when considering the Lorentz force. Therefore, one must restore magnetic contributions to the field fluctuations in order to employ a fully-retarded Green's function.

Energy-momentum conservation We briefly note that the arguments of the delta functions reflect energy-momentum conservation. In particular, the first delta function condition: $\omega'(1-\beta\cos\theta) - q_z v - \omega = 0$, must be satisfied in order for energy-momentum conservation to be satisfied in a process in which a polariton is absorbed and a photon is emitted. The second delta function condition $\omega'(1-\beta\cos\theta) - q_z v + \omega = 0$ must be satisfied in order for energy-momentum conservation to be satisfied in a process in which both the polariton and the photon are emitted.

To impose energy-momentum conservation in a compact way, we collect the energy and momentum of the incident and final particles into four-vectors, in which the first component is the energy and the other three components are the 3-momenta. The relevant momenta are:

$$\begin{aligned} p_i^\mu &= \left(\frac{E_i}{c}, \mathbf{p}_i\right) \\ p_f^\mu &= \left(\frac{E_f}{c}, \mathbf{p}_f\right) \\ k^\mu &= \hbar\left(\frac{\omega'}{c}, \mathbf{k}\right) \\ q^\mu &= \hbar\left(\frac{\omega}{c}, \mathbf{q}\right), \end{aligned} \tag{S16}$$

where $p_{i(f)}$ denotes the four-momentum of the initial (final) electron, k denotes that of the emitted photon, and q denotes that of the polariton. Here and henceforth, a Greek sub- or superscript denotes a four-vector. It is important to note that due to the evanescent nature of the polariton in the direction perpendicular to the polaritonic film, the momentum component in that direction is not a good quantum number of the polariton mode. Instead, it should be thought as variable, and sampled from a momentum probability distribution that roughly-speaking, is a squared Lorentzian. This squared Lorentzian form results from the fact that the momentum probability distribution for an evanescent wave would be the square of the Fourier transform of $e^{-q|z|}$, which is Lorentzian. When the incident electron moves in a direction with components along this direction, the variable momentum of the polariton in this direction broadens the phase space of emission. In the main text, we consider electrons moving parallel to a 2D plasmonic film. As a result, we will see that the effect of the momentum in transverse directions is essentially negligible.

The equation for conservation momentum in a process where a photon is emitted and a polariton is absorbed $(+)$ or emitted $(-)$ are:

$$p_i^\mu \pm q^\mu = p_f^\mu + k^\mu \tag{S17}$$

Squaring both sides of this equation, in the Minkowski sense, so that $a^\mu b_\mu = a_0 b_0 - \mathbf{a}\cdot\mathbf{b}$, we have that

$$\pm 2p_{i,\mu}q^\mu + q_\mu q^\mu = 2p_{f,\mu}k^\mu = 2(p_{i,\mu} \pm q_\mu - k_\mu)k^\mu = 2p_{i,\mu}k^\mu \pm 2q_\mu k^\mu \tag{S18}$$

where we have used that the square of any electron momentum is m^2c^2 and that the square of the momentum of a photon is zero. Further noting that for all situations considered in this text,

$\hbar\omega' \ll E_i$, $\hbar\omega \ll E_i$, $\hbar|\mathbf{k}| \ll |\mathbf{p}_i|$ and $\hbar|\mathbf{q}| \ll |\mathbf{p}_i|$, it follows that to leading order:

$$\pm p_{i,\mu} q^\mu = p_{i,\mu} k^\mu. \tag{S19}$$

Expanding the Minkowski dot products yields:

$$\pm(\omega - \mathbf{q}\cdot\mathbf{v}) = (\omega' - \mathbf{k}\cdot\mathbf{v}), \tag{S20}$$

with $\mathbf{v}$ the electron velocity. Taking this velocity to be in the arbitrarily chosen z-direction, and defining the angle of far-field photon emission θ to be relative to the z-direction, one immediately has that

$$\omega'(1 - \beta\cos\theta) \pm q_z v \mp \omega = 0. \tag{S21}$$

The $(-)$ branch of the equation $\omega'(1 - \beta\cos\theta) - q_z v + \omega = 0$, which describes emission, corresponds to the argument of delta function multiplying the $n_\omega + 1$ term, which is consistent with that term in Equation (S15) describing emission. The $(+)$ branch of the equation $\omega'(1-\beta\cos\theta)+q_z v-\omega = 0$, describes absorption of a polariton which is moving in the same direction as the electron. If the sign of q_z is flipped, it describes absorption of a polariton colliding head-on with the electron. Thus, in the argument of the delta function multiplying the n_ω term of Equation (S28), positive q_z corresponds to absorption of a polariton whose z-velocity is opposite that of the electron. Negative q_z, which is also included in the integration, corresponds to absorption of a plasmon whose z-velocity is in the same direction as that of the electron.

Emission spectrum for different materials and different material geometries In the main text, we show the result of Equation (S15) for the frequency spectrum associated with far-field emission of high energy photons. The only material-specific data needed to calculate the emission from

different materials is the p-polarized reflectivity. We consider three basic geometries: a semi-infinite slab geometry, a thin-film geometry, and a two-dimensional material geometry (such as graphene, which is considered in the main text (Figures 2 and 3)). In all cases, we consider the quasi-electrostatic limit of the expressions for the reflectivity, in keeping with the approximations that led to Equation (S9).

For an isotropic semi-infinite slab of permittivity $\epsilon(\omega)$ surrounded by vacuum, the p-polarized reflectivity is given by the simple expression:

$$r_p(\omega) = \frac{\epsilon(\omega) - 1}{\epsilon(\omega) + 1}. \tag{S22}$$

For a thin film of of permittivity $\epsilon(\omega)$ and thickness d surrounded by vacuum on the top side and a substrate of permittivity ϵ_s, the p-polarized reflectivity is given by:

$$r_p(q,\omega) = \left(\frac{\frac{\epsilon(\omega)-1}{\epsilon(\omega)+1} - \frac{\epsilon(\omega)-\epsilon_s}{\epsilon(\omega)+\epsilon_s} e^{-2qd}}{1 - \frac{\epsilon(\omega)-1}{\epsilon(\omega)+1}\frac{\epsilon(\omega)-\epsilon_s}{\epsilon(\omega)+\epsilon_s} e^{-2qd}} \right). \tag{S23}$$

For a two-dimensional material of surface conductivity $\sigma(\omega)$ surrounded by vacuum on the top side and a substrate of permittivity ϵ_s, provided that the mode wavelength is much longer than the thickness of the atomic layer, one has:

$$r_p(q,\omega) = \frac{(\epsilon_s - 1)i - \frac{q\sigma(\omega)}{\omega\epsilon_0}}{(\epsilon_s + 1)i - \frac{q\sigma(\omega)}{\omega\epsilon_0}}. \tag{S24}$$

As an example of a usage of the reflectivity of a monolayer, we use this in the results of the main text when considering plasmons in a sheet of graphene in the local limit modeled by a 2D Drude conductivity (with no dissipation).

In what follows, we discuss a few applications of Equations (S15) which both reaffirm and enrich the discussion and conclusions of the main text. We consider the influence of a finite Drude relaxation time, as well as the influence of interband damping[23,26]. We also discuss the power spectrum from alternative materials.

Influence of Drude relaxation and interband damping in graphene In Supplementary Figure 2, we calculate the emitted photon power per unit frequency of electromagnetic fluctuations in the surface. Integrating over frequency of fluctuations yields the total power emitted into high-frequency radiation, the kind of quantity we consider in Figure 4 of the main text. Unlike the discussion in the main text, we include a finite Drude relaxation time, which varies from 16 to 1600 fs, the longest value corresponding to observations reported in Ref.[27]. As one can see from Supplementary Figure 2, despite the fact that the relaxation time varies by three orders of magnitude, the intensity of emitted photons remains essentially the same.

In Supplementary Figure 3, we calculate the emitted photon power per unit frequency of electromagnetic fluctuations in the surface, but now for graphene modeled in the local and nonlocal RPA. For graphene modeled through either the local RPA or the non-local RPA (both giving similar results), there are additional contributions to the spectrum of fluctuations coming from interband transitions. Qualitatively, the main effect one sees in Supplementary Figure 3 is that below the Fermi frequency, the power spectrum is largely the same, with some red-shift of the peak (due to the plasmon red-shift in interband models), and some slight reduction of the peak in the nonlocal RPA case. Between the Fermi frequency and twice the Fermi frequency, the spectrum is reduced,

with the local RPA overestimating the extent of the dip. These behaviors are similar to those seen in previous work on Purcell enhancement of quantum emitters near graphene [23]. Above twice the Fermi frequency, there is a new contribution to the power which does not appear in the Drude model, which arises from electromagnetic fluctuations concomitant with interband damping (from the fluctuation-dissipation theorem). Unlike the Drude case, the emitted polariton above twice the Fermi frequency does not propagate, and thus the polaritonic character of the radiation is quite different at these frequencies.

Influence of different materials In Supplementary Figure 4, we consider the intensity of emitted photons induced by vacuum fluctuations in a different material. In particular, we consider the case of thin films of gold of varying thicknesses, whose permittivity we take to be of a Drude form, with parameters from[28]. We find that the emitted power is similar to that of graphene doped to a Fermi energy of 0.5 eV.

5 Simultaneous emission of a polariton and a high-energy photon in a fully quantum electrodynamical treatment

Note: In this section, we adopt (SI) natural units in which $\hbar = c = \epsilon_0 = 1$. These constants are restored in the final formulae (Equations (S45) and (S47)).

In this section, we present additional support for a duality between scattering from fluctuations and two-photon spontaneous emission. To do so, we consider a special case of the general phenomena above: an electron simultaneously emitting two quanta where one is a far-field photon

and the other is a plasmon in a two-dimensional electron gas. For simplicity, we assume that the electron is not so relativistic that it emits most of its energy into a single photon. This is a good approximation for electron energies above a fraction of a keV (covering possible experiments in electron microscopes), and stays relevant even for highly relativistic electrons with energies up to a few GeV (as in accelerator facilities, where the emitted photons carry much higher energies, yet still negligible relative to the electron energy). Having the emitted photon carrying a negligible part of the electron energy (also called the weak-recoil approximation) implies that we can model the interaction Hamiltonian via scalar QED. We now perform the calculations. We note first that the equivalence between the derivation in this section and the derivations of the previous section are not manifest until Equation (S44).

The scalar QED Hamiltonian is:

$$H_{int} = \int d^3x \; ieA^\mu(\psi^\dagger \partial_\mu \psi - (\partial_\mu \psi^\dagger)\psi) - e^2 A^\mu A_\mu |\psi|^2. \tag{S25}$$

Extremely relativistic electrons (> 5 GeV), may lose a significant part of their energy to the emission of a single photon through this process, thereby invalidating the use of scalar QED. In such scenarios, the interaction can be fully accounted for by considering the Dirac interaction Hamiltonian. The corresponding S-matrix, S_{fi} which describes transitions between initial states $|i\rangle$ and $|f\rangle$ is given by

$$S_{fi} = \langle f|\mathrm{T}\exp\left[\int d^4x \; eA^\mu(\psi^\dagger \partial_\mu \psi - (\partial_\mu \psi^\dagger)\psi) + ie^2 A^\mu A_\mu |\psi|^2\right]|i\rangle, \tag{S26}$$

with T being the time-ordering operator[29], and the metric is taken as $\mathrm{diag}(1,-1,-1,-1)$. A^μ is the quantized vector potential of the plasmons, and ψ is the field operator for the spinless electron

of scalar QED. It is written as an expansion over plane waves with four-momentum p in terms of the annihilation operator (c_p) for the electron and the creation operator for its anti-particle ($b_p^\dagger$) as $\psi = \int \frac{d^3p}{(2\pi)^3}\frac{1}{\sqrt{2E_p}}\left(e^{-ipx}c_p + e^{ipx}b_p^\dagger\right)$. Given the strong spatial confinement of the plasmons considered, we approximate its four-potential as a pure scalar potential Φ:

$$A^\mu = (\Phi, 0, 0, 0), \Phi = \sum_{\mathbf{q}} \sqrt{\frac{\omega_{\mathbf{q}}}{4qA}}\left(e^{i\mathbf{q}\cdot(y,z)-q|x|}a_{\mathbf{q}} + \text{h.c.}\right), \tag{S27}$$

with $\mathbf{q}$ being the plasmon wavevector, q being its magnitude, $\omega_{\mathbf{q}}$ being the wavevector-dependent plasmon frequency, and A being a normalization area.

Taking all terms in the expansion of the time-ordered exponential which are second-order in the electron charge, and plugging in the mode-expanded vector potential describing 2D Drude plasmons, we find that the emission rate Γ of a photon-polariton pair per unit photon solid angle Ω, per photon polarization, per unit plasmon frequency $\omega_{\mathbf{q}}$ and per unit plasmon propagation angle $\chi_{\mathbf{q}}$ is given by

$$\frac{d\Gamma}{d\Omega d\omega_{\mathbf{q}} d\chi_{\mathbf{q}}} = \frac{\alpha^2}{16\pi^3\bar{\epsilon}_r v_{g\mathbf{q}}(qL)(m\gamma)^2}\int_{-\infty}^{\infty}\frac{dQ}{(1+Q^2)^2}\frac{\omega_Q'^2\left|\hat{\epsilon}_k^\mu\hat{\epsilon}_q^\nu\left[\frac{(2p_\mu-2q_\mu)(2p_\nu-q_\nu)}{(p-q)^2-m^2}+\frac{(2p_\mu)(2p_\nu-q_\nu-2k_\nu)}{(p-k)^2-m^2}\right]\right|^2}{\beta n_{\mathbf{q}}\cos\chi_{\mathbf{q}} - 1 + \frac{\omega_{\mathbf{q}}}{2m\gamma}(1-n_{\mathbf{q}}^2(1+Q^2))}, \tag{S28}$$

where ω_Q' is defined as:

$$\omega_Q' = \omega_{\mathbf{q}}\frac{\beta n_{\mathbf{q}}\cos\chi_{\mathbf{q}} - 1 + \frac{\omega_{\mathbf{q}}}{2m\gamma}(1-n_{\mathbf{q}}^2(1+Q^2))}{1-\beta\cos\theta + \frac{\omega_{\mathbf{q}}}{m\gamma}(n_{\mathbf{q}}\cos\chi_{\mathbf{q}}\cos\theta + n_{\mathbf{q}}\sin\chi_{\mathbf{q}}\sin\theta\sin\phi + n_{\mathbf{q}}Q\sin\theta\cos\phi - 1)}. \tag{S29}$$

In these equations $\alpha = \frac{e^2}{4\pi}$ is the fine-structure constant with e the electron charge, m is the electron mass, β is the electron's initial speed, γ is the corresponding Lorentz factor, ω' is the frequency of the emitted photon, $\bar{\epsilon}_r$ is the average permittivity surrounding the 2D electron gas (which in terms

of the substrate permittivity ϵ_s is $\frac{1+\epsilon_s}{2}$), $v_{g\mathbf{q}}$ is the group velocity of the plasmon, $\hat{\epsilon}_k^\mu$ is the polarization of the emitted photon, $\hat{\epsilon}_{\mathbf{q}}^\mu$ is the polarization of the plasmon four-potential, given by $(1,0,0,0)$ as we describe the plasmon by a scalar potential. This corresponds to an electric-field polarization of $\frac{\hat{q}+i\hat{x}}{\sqrt{2}}$ (hats denote unit vectors). Meanwhile, $n_{\mathbf{q}} = \frac{qc}{\omega_{\mathbf{q}}}$ is the confinement factor of effective mode-index of the plasmon, p^μ is the four-momentum of the electron, q^μ is the four-momentum of the plasmon, and k^μ is the four-momentum of the radiated photon. The four-momentum of the plasmon is parameterized as $q^\mu = \omega_{\mathbf{q}}(1, n_{\mathbf{q}}Q, n_{\mathbf{q}}\sin\chi_{\mathbf{q}}, n_{\mathbf{q}}\cos\chi_{\mathbf{q}})$, with Q a dimensionless integration variable proportional to the momentum of the plasmon transverse to the 2D sheet[1]. From this parameterization, $\chi_{\mathbf{q}}$ is the angle of plasmon emission with respect to the projection of the electron's initial velocity vector in the plane of the 2D sheet.

Making a weak recoil approximation by expanding the denominators to lowest non-trivial order in $\frac{\omega_{\mathbf{q}}}{m}$, we find that the Q-integration gives (after summing over photon polarizations)

$$\frac{2\pi n_{\mathbf{q}}^2\omega_{\mathbf{q}}^2}{(1-\beta\cos\theta)^2(\beta n_{\mathbf{q}}\cos\chi_{\mathbf{q}}-1)}F(\theta,\phi,\chi_{\mathbf{q}}), \tag{S30}$$

where

$$\begin{aligned}F(\theta,\phi,\chi_{\mathbf{q}}) =& \sin^2\phi + \sin^2\chi_{\mathbf{q}}\cos^2\phi \\ &+ \frac{(\sin\chi_{\mathbf{q}}\sin\phi(\cos\theta-\beta) - \frac{1}{\gamma^2}\sin\theta\cos\chi_{\mathbf{q}})^2 + \cos^2\phi(\cos\theta-\beta)^2}{(1-\beta\cos\theta)^2}.\end{aligned} \tag{S31}$$

[1]Note that the integration goes only over Q that yield a positive output photon frequency. Denote this maximum possible Q as Q_m. However, the squared Lorentzian in practice gives all of its contributions to the integration at a maximum $Q \ll Q_m$, meaning that we can extend the limits of integration to ∞.

Multiplying by the emitted photon energy ω to get the power emitted, we have that

$$\frac{dP}{d\Omega_k} = \int \frac{d^2q}{(2\pi)^2} \frac{\alpha^2 q \omega_{\mathbf{q}}}{2\bar{\epsilon}_r m^2 \gamma^2 (1-\beta\cos\theta)^3} \frac{1}{(qL)} F(\theta, \phi, \chi_{\mathbf{q}}), \tag{S32}$$

We note that the factor $(qL)^{-1}$ is essentially the average over the electron length L of the exponential tail of the plasmon in the limit of $qL \gg 1$. In particular, $\frac{1}{L}\int_{-L/2}^{L/2} dx\, e^{-2q|x|} = \frac{1}{qL}$. As a result, if electron is treated as a point electron centered at transverse distance x_0 away from the plasmonic sheet, the factor $(qL)^{-1}$ is replaced by e^{-2qx_0}. In the case of a Gaussian wavepacket that resembles a point charge one would get a similar result. We now consider this case in order to make close contact with the previous sections of the paper.

Effects of fermionic electrodynamics In this section, we consider the effect of the fermionic nature of the electron on the radiation spectrum associated with photon-polariton pair emission. The interaction Hamiltonian between a Dirac fermion and the electromagnetic field is given by:

$$H_{int} = e \int d^3x\, \bar{\psi}(x) \gamma_\mu A^\mu(x) \psi(x). \tag{S33}$$

The fermion field operator ψ is given by[29]:

$$\psi(x) = \int \frac{d^3p}{(2\pi)^3} \sum_{\text{spins},s} \frac{1}{\sqrt{2E_p}} \left(e^{-ip_\mu x^\mu} u_{p,s} c_{p,s} + e^{ip_\mu x^\mu} v_{p,s} b^\dagger_{p,s} \right), \tag{S34}$$

where, p_μ is a four-momentum, E_p is the energy of a fermion with four-momentum p, $c_{p,s}(b_{p,s})$ is an annihilation operator for the electron (positron), and $u_{p,s}(v_{p,s})$ is the corresponding spinor for the electron (positron). The field operator $\bar{\psi}$ is related to ψ by $\bar{\psi} = \psi^\dagger \gamma^0$ with γ^0 being the time-component of the vector of gamma matrices γ^μ with $\gamma^0 = \text{diag}(1, 1, -1, -1)$ in the particular represention we choose (Dirac representation). The spinors in the representation we choose are

given by[30]

$$u_p^s = \begin{pmatrix} \sqrt{E_p + m}\,\eta^s \\ \frac{\mathbf{p}\cdot\sigma}{\sqrt{E_p+m}}\eta^s \end{pmatrix} \tag{S35}$$

with $\eta^s = (1, 0)$ for spin-up and $(0, 1)$ for spin-down.

To calculate the analogous radiation emission $\frac{d\Gamma}{d\Omega d\omega_{\mathbf{q}} d\chi_{\mathbf{q}}}$ of Equation (S28), it is sufficient simply to replace the absolute square in the numerator of the integrand of Equation (S28) by

$$\left| \bar{u}_{r,s'} \hat{\epsilon}_k^\mu \hat{\epsilon}_q^\nu \left[\frac{\gamma_\mu (\not{p} - \not{q} + m)\gamma_\nu}{(p-q)^2 - m^2} + \frac{\gamma_\nu (\not{p} - \not{k} + m)\gamma_\mu}{(p-k)^2 - m^2} \right] u_{p,s} \right|^2, \tag{S36}$$

where we are making use of the Feynman slash notation: $\not{A} = \gamma_\mu A^\mu$.

For low electron energies, such that the radiated photon carries only a small fraction of the electron's energy, the scalar treatment of the electron accurately captures the radiation spectrum. This is shown in Supplementary Figure 5, where we compare the spectrum predicted by fermionic quantum electrodynamics and scalar quantum electrodynamics. In particular, we show $S(\theta, \phi, \omega, \chi) = \frac{dP}{d\Omega d\omega d\chi}$ for spontaneous emission of a photon and a plasmon. The plasmon is taken to have an energy of 0.5 eV, the Fermi level is also taken to be 0.5 eV, and the plasmon is taken to be emitted in the forward direction. We plot the spectrum as a function of the photon polar angle (the azimuthal angle is taken to be zero). The electron is taken to be 5 nm away from the graphene surface. As can be seen from the figure, even for electron energies as high as 300 MeV, corrections due to the fermionic nature of the electron are weak. The contribution to the radiation spectrum from transitions that conserve the spin of the electron is nearly identical to the radiation spectrum predicted within scalar QED. Moreover, the contribution to the radiation spectrum from transitions

that change the electron spin are about 0.1% of the total radiation for electrons of 300 MeV energy. For electrons of 3 GeV energy, as in panel (c), spin-changing contributions become comparable to spin-conserving contributions, but are still significantly weaker. The spin conserving contribution to the spectrum also differs somewhat from the spectrum predicted by scalar QED.

Equivalence to the fluctuational theory In this section, we demonstrate the equivalence of the fluctuational theory of Sections 3 and 4, and the relativistic quantum field theory of this section.

Consider Equation (S15) for the case of a 2D electron gas described by a Drude model. In that case, the imaginary part of the p-polarized reflectivity can be shown[24] to be given by Im $r_p(q,\omega) = \frac{\pi}{\bar{\epsilon}_r} q v_{g\mathbf{q}} \delta(\omega - \omega_{\mathbf{q}})$, where $\omega_{\mathbf{q}} \sim \sqrt{q}$ is the dispersion relation. Plugging this form in, and integrating over the photon frequency ω, one finds that

$$\frac{dP}{d\Omega} = \frac{\alpha^2 \hbar^3}{\bar{\epsilon}_r m^2 \gamma^2 c (1 - \beta \cos\theta)^5} \int \frac{d^2q}{(2\pi)^2}\, q\omega_{\mathbf{q}} |\mathbf{T}\hat{\epsilon}_\gamma(\chi_{\mathbf{q}})|^2 e^{-2qx_0}. \tag{S37}$$

Using the equivalence $\frac{1}{2}(1 - \beta\cos\theta)^2 F(\theta,\phi,\chi) = |\mathbf{T}\hat{\epsilon}_\gamma(\chi_{\mathbf{q}})|^2$, it follows immediately that Equations (S32) and (S37) are equal (note (S32) is in natural units), for the case of a point electron, verifying for the specific case of a 2D Drude sheet the equivalence of the fluctuational and quantum field-theoretic derivations of spontaneous emission of a photon-polariton pair. A similar equivalence is going to be found for other structures as well.

Total power emitted We now integrate over the angular spectrum to retrieve the total power emitted into high-energy photons in this photon-polariton pair emission process. Taking Equation (S32) as appropriate for a point electron, and keeping in mind that the integration limits for $\chi_{\mathbf{q}}$ are

$\pm\frac{\pi}{2}$ in the limit of highly confined plasmons, the net power obtained is

$$P = \frac{e^4\gamma^2(4-\beta)^2}{24\pi m^2}\left(\int \frac{dq}{2\pi}\frac{\omega_{\mathbf{q}}q^2}{2\bar{\epsilon}_r}e^{-2qx_0}\right) \tag{S38}$$

Noting that the remaining integral in parentheses is $\langle 0|\mathbf{E}^2|0\rangle$, the expectation value in the vacuum state of the electric field operator describing the plasmon, one arrives at (now in SI units)

$$P = \frac{e^4\gamma^2(4-\beta^2)}{24\pi\epsilon_0 m^2c^3}\langle 0|\mathbf{E}^2|0\rangle. \tag{S39}$$

In the relativistic limit, the field which modulates the electron is not precisely $\langle 0|\mathbf{E}^2|0\rangle$ but instead it is $\langle 0|\mathbf{E}_\gamma^2|0\rangle$, which is less than $\langle 0|\mathbf{E}^2|0\rangle$ by a factor of $3/4$ in the relativistic limit. Expressing Equation (S39) in the relativistic limit, noting also that $4-\beta^2 \approx 3$, we have that (in SI units)

$$P \approx \frac{e^4\gamma^2}{6\pi\epsilon_0 m^2c^3}\langle 0|\mathbf{E}_\gamma^2|0\rangle. \tag{S40}$$

See further discussion about this equivalence and its consequences in the main text.

1. Popmintchev, T. *et al.* Bright coherent ultrahigh harmonics in the kev x-ray regime from mid-infrared femtosecond lasers. *Science* **336**, 1287–1291 (2012).

2. Pizzi, A. *et al.* Graphene metamaterials for intense, tunable and compact euv and x-sources. In *CLEO: QELS Fundamental Science*, FW4H–7 (Optical Society of America, 2018).

3. Graves, W., Kärtner, F., Moncton, D. & Piot, P. Intense superradiant x rays from a compact source using a nanocathode array and emittance exchange. *Physical review letters* **108**, 263904 (2012).

4. Nanni, E. A., Graves, W. S. & Moncton, D. E. Nanomodulated electron beams via electron diffraction and emittance exchange for coherent x-ray generation. *Physical Review Accelerators and Beams* **21**, 014401 (2018).

5. Naumova, N. *et al.* Attosecond electron bunches. *Physical review letters* **93**, 195003 (2004).

6. Lim, J., Chong, Y. & Wong, L. J. Terahertz-optical intensity grating for creating high-charge, attosecond electron bunches. *New Journal of Physics* **21**, 033020 (2019).

7. Wong, L. J., Kaminer, I., Ilic, O., Joannopoulos, J. D. & Soljačić, M. Towards graphene plasmon-based free-electron infrared to x-ray sources. *Nature Photonics* **10**, 46–52 (2016).

8. Brinkmann, R., Derbenev, Y. & Flöttmann, K. A low emittance, flat-beam electron source for linear colliders. *Physical Review Special Topics-Accelerators and Beams* **4**, 053501 (2001).

9. Piot, P., Sun, Y.-E. & Kim, K.-J. Photoinjector generation of a flat electron beam with transverse emittance ratio of 100. *Physical Review Special Topics-Accelerators and Beams* **9**, 031001 (2006).

10. Ody, A. *et al.* Flat electron beam sources for dla accelerators. *Nuclear Instruments and Methods in Physics Research Section A: Accelerators, Spectrometers, Detectors and Associated Equipment* **865**, 75–83 (2017).

11. Lui, C. H., Liu, L., Mak, K. F., Flynn, G. W. & Heinz, T. F. Ultraflat graphene. *Nature* **462**, 339–341 (2009).

12. Fei, Z. *et al.* Electronic and plasmonic phenomena at graphene grain boundaries. *Nature nanotechnology* **8**, 821–825 (2013).

13. Deng, S. & Berry, V. Wrinkled, rippled and crumpled graphene: an overview of formation mechanism, electronic properties, and applications. *Materials Today* **19**, 197–212 (2016).

14. Leong, W. S. *et al.* Paraffin-enabled graphene transfer. *Nature communications* **10**, 867 (2019).

15. Jackson, J. D. *Classical Electrodynamics* (Wiley, 1999).

16. Landau, L. D. & Lifshitz, E. M. *The Classical Theory of Fields* (Pergamon, 1971).

17. Rytov, S., Kravtsov, Y. A. & Tatarskii, V. *Priniciples of Statistical Radiophysics. 3. Elements of Random Fields.* (Springer, 1989).

18. Joulain, K., Mulet, J.-P., Marquier, F., Carminati, R. & Greffet, J.-J. Surface electromagnetic waves thermally excited: Radiative heat transfer, coherence properties and casimir forces revisited in the near field. *Surface Science Reports* **57**, 59–112 (2005).

19. Volokitin, A. & Persson, B. N. Near-field radiative heat transfer and noncontact friction. *Reviews of Modern Physics* **79**, 1291–1329 (2007).

20. Rodriguez, A. W., Capasso, F. & Johnson, S. G. The casimir effect in microstructured geometries. *Nature Photonics* **5**, 211–221 (2011).

21. Novotny, L. & Hecht, B. *Principles of nano-optics* (Cambridge university press, 2012).

22. Scheel, S. & Buhmann, S. Y. Macroscopic quantum electrodynamics: concepts and applications. *Acta Phys. Slovaca* **58**, 675–809 (2008).

23. Koppens, F. H., Chang, D. E. & García de Abajo, F. J. Graphene plasmonics: a platform for strong light–matter interactions. *Nano Letters* **11**, 3370–3377 (2011).

24. Rivera, N., Kaminer, I., Zhen, B., Joannopoulos, J. D. & Soljačić, M. Shrinking light to allow forbidden transitions on the atomic scale. *Science* **353**, 263–269 (2016).

25. Chang, C.-H., Rivera, N., Joannopoulos, J. D., Soljacic, M. & Kaminer, I. Constructing "designer atoms" via resonant graphene-induced lamb shifts. *ACS Photonics* **4**, 3098–3105 (2017).

26. Jablan, M., Buljan, H. & Soljačić, M. Plasmonics in graphene at infrared frequencies. *Physical review B* **80**, 245435 (2009).

27. Ni, G. *et al.* Fundamental limits to graphene plasmonics. *Nature* **557**, 530–533 (2018).

28. Johnson, P. B. & Christy, R.-W. Optical constants of the noble metals. *Physical review B* **6**, 4370–4379 (1972).

29. Peskin, M. E. *An introduction to quantum field theory* (Westview press, 1995).

30. Berestetskii, V. B., Landau, L. D., Lifshitz, E. M. & Pitaevskii, L. *Quantum electrodynamics*, vol. 4 (Butterworth-Heinemann, 1982).